

Accelerated Stress Test Assessment of Through-Silicon Via Using RF Signals

Chukwudi Okoro, Pavel Kabos, Jan Obrzut, Klaus Hummler, and Yaw S. Obeng

Abstract—In this paper, radio frequency signal is demonstrated as an effective probe for assessing the effect of thermal cycling on the reliability of through-silicon vias (TSVs) in stacked dies. It is found that the RF signal integrity in TSV daisy chain, particularly its transmission characteristics, degrades considerably with extended thermal cycling, because of the formation and the growth of voids. Early failures are observed in the reliability analysis of the TSV daisy chain and are attributed to processing-related variability across the wafer. However, the maximum failure rate is found to occur at 500 thermal cycles, which is attributed to the initiation of defects and their subsequent propagation.

Index Terms—Failure analysis, radio-frequency (RF), thermal cycling, through-silicon via (TSV).

I. INTRODUCTION

RECENTLY, 3-D stacking of chips achieved by using through-silicon vias (TSVs) has gained much attention, as it enables improved system miniaturization and higher system performance. This is due to its short wiring path, high interconnect density, and its smaller foot print as compared with the conventional multichip modules [1]. Because of the complexity associated with the integration of TSVs, most studies conducted so far have focused on solving the processing-related concerns plaguing its adoption. The challenges include the following: 1) copper-pumping [2]; 2) electrodeposition of Cu [3]; 3) wafer thinning and bonding [4]; 4) TSV proximity to transistors [5]; and 5) stress/strain characterization [6] and much more. Recently, studies on TSV reliability are reported in the fields of electromigration [7] and thermal cycling [8], [9]. All the reported studies are performed using the direct current (dc) resistance (R_{dc}) measurement technique.

A study performed on solder joint reliability has demonstrated that the use of R_{dc} in reliability studies results in late or delayed prognostics in comparison with the use of

radio frequency (RF) signals [10]. Independently, the RF-based approach is demonstrated to be sensitive to the degree of void damage in metal lines in back-end-of-line interconnect reliability studies [11]. These two studies suggest that RF-based measurement technique can also be applied to TSV reliability studies.

The use of RF-based measurement techniques offers many advantages over the R_{dc} technique. Firstly, the performance of interconnects can be studied over a broad frequency range, which is not possible with the R_{dc} technique. Broad frequency range reliability analyses of TSVs are essential as TSV-based chips will find application in a variety of devices with operating frequencies in the GHz range. Secondly, the R_{dc} technique is only sensitive to discontinuities/distortion in the conductive paths. For interconnects, especially TSVs, it is also important to detect changes not only limited to the conductive paths, but also in the surrounding barrier (Ta/TaN) and isolation liners (SiO_2), as well as at their interfaces. This can only be achieved through the RF-based techniques. Thirdly, the R_{dc} techniques measures only signal transmission. On the other hand, the RF-based technique measures both the reflection and the transmission of signals, as well as signal phases, which provides more complete information about the character of the response. In addition, the broadband approach allows for the detection and identification of potential problems within the TSV/TSV chain that cannot be detected by R_{dc} measurements.

Indeed, some recent studies have used RF-based techniques to monitor TSV performance, by evaluating changes in their impedance [12]–[14]. The primary objective of those studies is to develop optimum conditions for TSV design. These studies are conducted on as-fabricated state, without applying thermal stress to the TSVs.

In this paper, probing with RF signals, up to 40 GHz, is used as a prognostic tool for the assessment of the impact of thermal cycling on the performance of Cu TSVs. Additionally, physical failure analysis is performed using the focused ion beam (FIB) technique to cross section a subset of the test samples for microscopy.

II. SAMPLE AND EXPERIMENT DESCRIPTION

A. Samples

For the current study, two-level stacked dies provided by SEMATECH¹ are used. The TSVs are nominally $5.5\mu\text{m}$ in

¹Certain commercial equipment, instruments, or materials are identified in this paper to specify experimental or theoretical procedures. Such identification does not imply recommendation by NIST nor the authors, nor does it imply that the equipment or materials are necessarily the best available for the intended purpose.

Manuscript received November 19, 2012; revised March 29, 2013; accepted April 1, 2013. Date of current version May 16, 2013. The review of this paper was arranged by Editor B. Kaczer.

C. Okoro and Y. S. Obeng are with the Department of Semiconductor and Dimensional Metrology Division, National Institute of Standards and Technology, Gaithersburg, MD 20899 USA (e-mail: chukwudi.okoro@nist.gov; yaw.obeng@nist.gov).

P. Kabos is with the Department of Electromagnetics Division, National Institute of Standards and Technology, Boulder, CO 80305 USA (e-mail: pavel.kabos@nist.gov).

J. Obrzut is with the Department of Material Science and Engineering Division, National Institute of Standards and Technology, Gaithersburg, MD 20899 USA (e-mail: jan.obrzut@nist.gov).

K. Hummler is with the Department of 3D Integration, SEMATECH, Albany, NY 12203 USA (e-mail: klaus.hummler@sematech.org).

Color versions of one or more of the figures in this paper are available online at <http://ieeexplore.ieee.org>.

Digital Object Identifier 10.1109/TEDE.2013.2257791

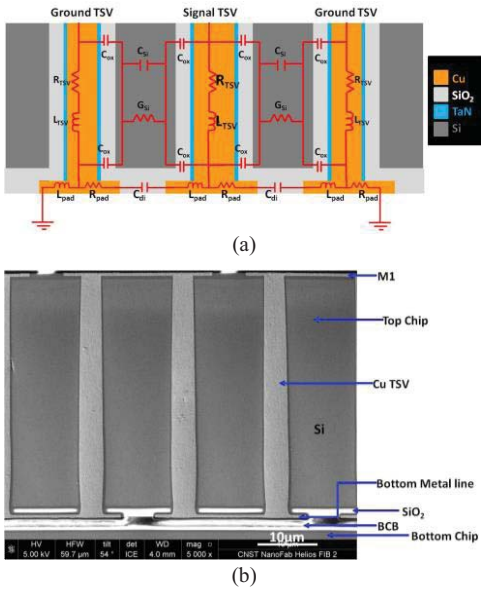


Fig. 1. (a) Schematic representation of the top chip and its circuit diagram, having a ground-signal-ground (GSG) TSV configuration. (b) SEM cross-sectional image of the stacked chip, showing the signal TSV daisy chain.



Fig. 2. Top-view image of the RF test structure used in this paper, having a GSG configuration.

diameter and $50\text{-}\mu\text{m}$ deep and are located at the top chip. The top and the bottom chips are bonded together with benzocyclobutene. Scanning electron microscopy (SEM) and schematic images of the test structure are shown in Fig. 1. Top metallization (M1) is not passivated.

The different electrical elements in the circuit diagram shown in Fig. 1(a) are defined as: 1) TSV resistance (R_{TSV}); 2) Cu-landing pad resistance (R_{pad}); 3) TSV inductance (L_{TSV}); 4) Cu-landing pad inductance (L_{pad}); 4) isolation liner capacitance (C_{ox}); 5) Si substrate capacitance (C_{Si}); 6) damascene SiO_2 capacitance (C_{di}); and 7) Si substrate conductance (G_{Si}).

The thicknesses of the isolation liner (SiO_2), the barrier layer (TaN), and the damascene SiO_2 thickness are 0.5 , 0.025 , and $2\ \mu\text{m}$, respectively. The conductivity of the Si substrate is estimated to be $18\ \Omega\cdot\text{cm}$.

The studied RF test structure is a daisy chain of 60 TSVs with pitch size of $16\ \mu\text{m}$. This test structure has a GSG configuration, which means that it has three parallel rows of TSVs, $15\ \mu\text{m}$ apart, each having a daisy chain of 60 TSVs that are terminated at both ends to probe pads as shown in Fig. 2. Based on time-domain reflectometer measurements, the low-frequency characteristic impedance of the TSV daisy chain is determined to be $\sim 45\ \Omega$.

B. Experiment

The RF test structures are first measured in the as-received state, prior to any thermal cycling, to determine their baseline

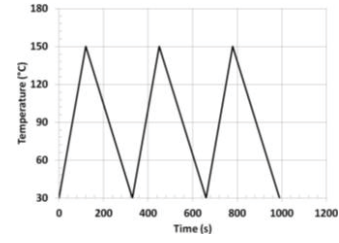


Fig. 3. Schematic representation of the used thermal-cycling profile.

RF signal characteristics. Thereafter, the test structures are subjected to thermal cycling. The thermal-cycling profile used in this paper is shown in Fig. 3, where the sample is heated from $30\ \text{°C}$ to $150\ \text{°C}$ and then cooled back to $30\ \text{°C}$ in laboratory conditions. Each cycle is completed in 5.5 min. This temperature profile is chosen to mimic the environmental conditions that a typical chip will experience in service. RF measurements are performed every 500 thermal cycles, for up to a maximum of 2000 thermal cycles. All measurements are performed at room temperature.

In this paper, a vector network analyzer (VNA), PNA N5230A is used as the RF generator and analyzer.¹ The VNA, cables, and probes are calibrated using WinCal Xe software and an ISS-101-190 impedance calibration substrate.¹ A two-port measurement is performed, and both the magnitude and the phase of the frequency-dependent four component scattering parameters (S_{11} , S_{12} , S_{21} , and S_{22}) of the TSV chain are obtained. The scattering parameter (or S-parameter) is a matrix that quantifies how RF energy propagates through a multiport network. Thirty-four samples, from a single wafer are used in this paper.

Analysis of the RF data is performed, to determine the failure characteristics of the TSV daisy chain samples. In this paper, a 20% degradation of the transmission coefficient magnitude is used as the failure criterion [15]. The baseline transmission coefficient magnitude data used as the reference for failure criterion definition is derived by taking the arithmetic mean of the transmission coefficient magnitude data of the 34 as-received samples. The samples that meet the failure criterion are withdrawn from the sample pool; thus, the total number of test samples decrease with increasing number of thermal cycles.

Cross-sectional SEM images of the top region of the TSV and its connecting metal line (M1) are taken immediately following the FIB milling for the as-received and 1000 thermal cycle test conditions. In performing the failure analysis, we pay particular attention to the presence of defects in and around the TSVs.

III. RESULTS AND DISCUSSION

A. RF-Based

Figs. 4 and 5 show the RF results of a single sample, as a function of its thermal history. The change in the magnitude of the transmission coefficient and the reflection coefficient, as a function of thermal cycling and frequency are shown in Fig. 4(a) and (b), respectively. From Fig. 4(a), the measured transmission coefficient magnitude degraded with thermal

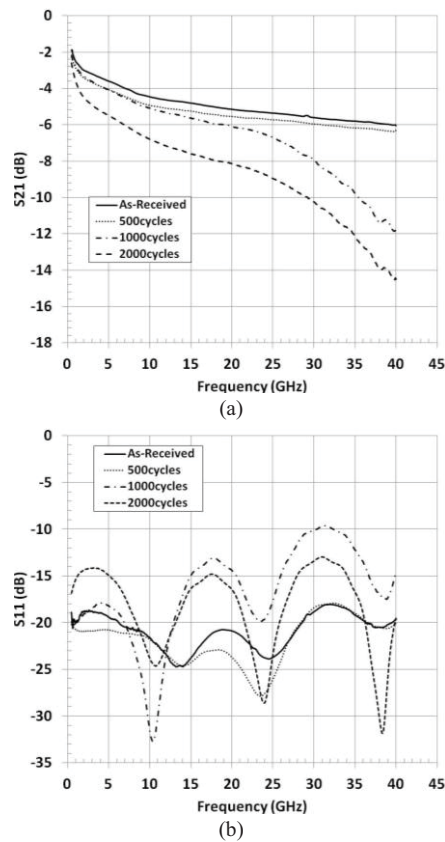


Fig. 4. Effect of thermal cycling on the magnitude of (a) transmission coefficient and (b) reflection coefficient.

cycling. For instance, at 20 GHz the transmission coefficient magnitude changed from an original value of 5.2 dB to 5.6 dB after 500 thermal cycles. Upon further cycling to 1000 and 2000 thermal cycles, the transmission coefficient magnitude deteriorated further to 6.0 dB to 8.0 dB, respectively. Additionally, thermal cycling is observed to affect the frequency characteristics of the magnitude of the transmission coefficient. The RF characteristics of the as-received and the 500-cycled test conditions are shown to be similar, with a constant 0.4 dB decrease in the transmission coefficient magnitude across all frequencies upon thermal cycling to 500 cycles. However, the 1000 and 2000 thermal-cycled data show a significantly different trend in comparison with the as-received state; the transmission coefficient magnitude deteriorated rapidly with increasing frequency. This trend further worsens > 20 GHz for 1000 and higher number of thermal cycles. This indicates that for 1000 and higher number of thermal cycles, that the signal integrity in TSVs for applications operating > 20 GHz are anticipated to be unreliable. This conclusion could not be obtained from dc resistivity measurements.

Fig. 4(b), shows the effect of thermal cycling on the magnitude of the reflection coefficient. No clear thermal-cycling effect is observed across all frequencies. For instance, at 20 GHz, before thermal cycling, the magnitude of the S_{11} is 21.0 dB, upon cycling to 500 thermal cycles, its S_{11} magnitude becomes 23.5 dB, representing an improvement of ~ 2.5 dB. After 1000 thermal cycles, the reflection coefficient magnitude degraded to 14.3 dB, only to improve to 16.3 dB after 2000

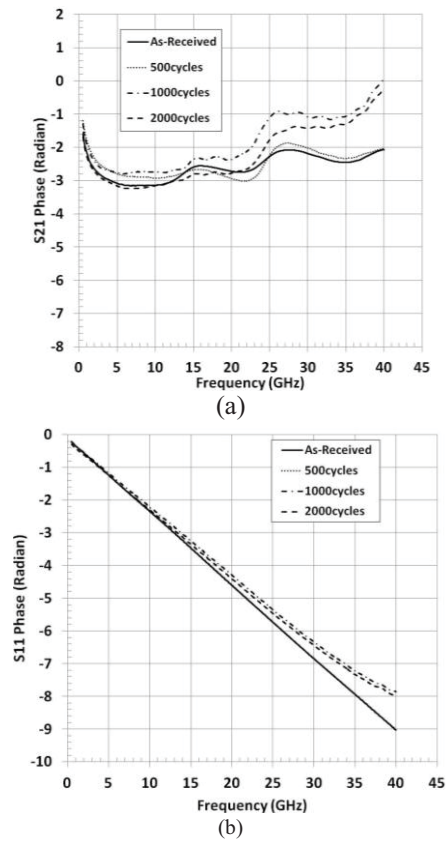


Fig. 5. Effect of thermal cycling on the phase angle characteristics of (a) transmission coefficient and (b) reflection coefficient.

thermal cycles. This means that the effect of thermal cycling on the performance of TSVs cannot be easily convoluted from the magnitude of the reflection coefficient, as opposed to the transmission coefficient magnitude shown in Fig. 4(a). This also indicates that the main cause of the degradation of the transmission coefficient magnitude with thermal cycling is not due to signal reflection. The RF signal losses in the TSV can be attributed to changes in material properties, and changes in structure, resulting from the thermal-cycling process. The reflection data (S_{11}) magnitude data show that the TSVs are relatively well matched.

Considering, the transmission and reflection coefficient magnitude data in Fig. 4, suggest that postprocessing thermal cycling to 500 cycles optimizes the RF performance of this TSV daisy chain. The losses do not deteriorate significantly in the whole frequency range and the thermal cycling improves the impedance matching of the TSV's. Although this is true for this single sample, statistical analysis (Figs. 6 and 8) based on 34 samples, discussed below, paints a different picture.

The phase angle results of the transmission coefficient and the reflection coefficient are presented in Fig. 5(a) and (b), respectively. From Fig. 5(a), it is observed that phase angle of the transmission coefficient after 1000 and 2000 thermal cycles, begins to drastically increase > 15 GHz. This increase in the S_{21} phase angle > 15 GHz, is related to the change of the impedance of the structure because of the increased damping and change of the permittivity of the structure. This is consistent with the structural changes in the materials,

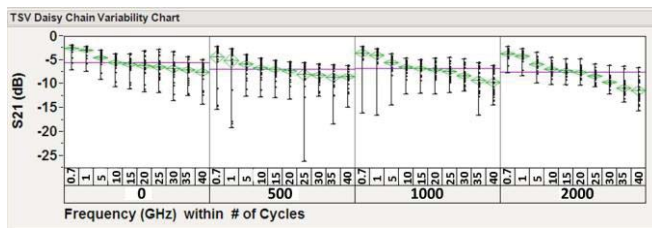


Fig. 6. Analysis of the effect of thermal cycles on the magnitude of the transmission coefficient (S_{21}) as a function of frequency. The reported error bars: \pm three times the standard deviation of the 34 samples that are measured. The variability is a composite of sample-to-sample variability and systematic experimental variability as discussed in text.

discussed above. This could be a possible indication of the formation of voids or the occurrence of delamination in the structure caused by the buildup of stresses because of the thermal-cycling process.

The frequency dependence of the phase angle of the reflection coefficient shown in Fig. 5(b), confirms the trend observed in transmission data, albeit, not in a straightforward way.

From all these studies shown in Figs. 4 and 5, it follows that the frequency dependence of the magnitude and/or phase of the transmission coefficient show/shows clear dependence of RF signal characteristics on thermal cycling. Therefore, all the succeeding RF-based studies presented in this paper will be based on the transmission coefficient magnitude results.

In Fig. 6, statistical variability analysis is performed on 34 die samples taken from the same wafer. In this representation, the middle lines of the diamonds represent the arithmetic mean, whereas the top and bottom apexes represent the 95% confidence intervals of the cell data. Thus, the horizontal lines in the graphs represent the grand mean transmission coefficient magnitude, which is used to compare the difference in the transmission coefficient magnitude as a function of the number of thermal cycles.

From these horizontal lines, it is observed that the average transmission coefficient magnitude before thermal cycling is ~ 5.5 dB. After 500 thermal cycles the average transmission coefficient magnitude is observed to have decreased to 7.5 dB, representing a 2.0-dB worsening of the transmission coefficient magnitude. The RF signal characteristic remains constant upon further thermal cycling to 1000 cycles; the transmission coefficient magnitude values at 500 and 1000 cycles are observed to be comparable. However, thermal cycling to 2000 cycles result in a further 0.8-dB worsening of the transmission coefficient magnitude.

Analysis of the total change in the transmission coefficient magnitude from 0.7 to 40 GHz for the different test conditions results in 5.0, 5.0, 5.7, and 8.0 dB, respectively, for the as-received, 500, 1000, and 2000 thermal cycles test conditions. This trend is in agreement with Fig. 4(a), which shows that for 1000 thermal cycles and above, the RF signal integrity in TSVs drastically worsens, especially > 20 GHz. Thus, further analyses presented in this paper are limited to a maximum frequency of 20 GHz.

To better visualize the changes in the RF signal characteristics with thermal cycling, the transmission coefficient magnitude value of a sample after a given number of thermal

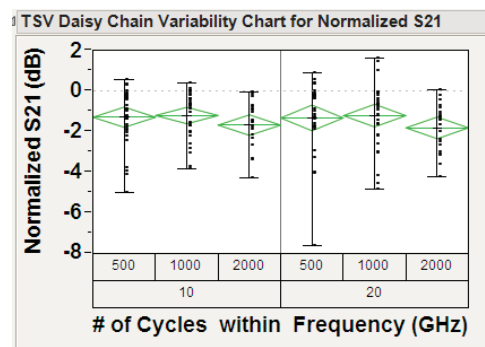


Fig. 7. Variability analysis of the normalized magnitude of the transmission coefficient (S_{21}) data as a function of the number of thermal cycles, at 10 and 20 GHz frequencies. The reported error bars: \pm three times the standard deviation of the measured samples. The shown variability is a composite of sample-to-sample variability and systematic experimental variability.

cycles is normalized to its value before thermal cycling. The ratio, plotted in Fig. 7, shows the relative increase in the damping of the RF test structure at the given frequencies (10 and 20 GHz). Using the arithmetic mean as a yardstick, this graph follows a similar trend as Fig. 6, as the main changes in the RF characteristics occurred at 500 and 2000 cycles for both 10 and 20 GHz frequencies. On the other hand, the least change is observed at 1000 cycles.

The degradation in the magnitude of the transmission coefficient with thermal cycling, shown in Figs. 4(a), 6, and 7, is attributed to the increase in discontinuities/defects in the TSV daisy chain structure. These defects arise from the thermal-cycling process, which results in the buildup of stress in the TSV daisy chains. This occurs because of the confinement and the mismatch in the coefficient of thermal expansion of Cu (16.7 ppm/ $^{\circ}$ C), SiO₂ isolation liner (0.5 ppm/ $^{\circ}$ C), and the surrounding Si matrix (2.3 ppm/ $^{\circ}$ C) [6], leading to stress buildup, and subsequently leading to the formation and growth of voids, as well as possible delamination at interfaces [16]. The formed defects act as scattering centers for RF signals, resulting in the lower transmission coefficient magnitude with thermal cycling.

At 20 GHz and below, the magnitude of the transmission coefficient is observed to be approximately constant from 500 to 1000 thermal cycles. This trend is even more pronounced in Fig. 7, where the average change in the RF characteristics at 1000 cycles is observed to have the same transmission coefficient magnitude values at 10 and 20 GHz frequencies. This indicates that at 20 GHz and below, the failure mechanism at play stabilizes from 500 to 1000 thermal cycles, thus resulting in the observed constant magnitude of the transmission coefficient. However, at 2000 cycles the transmission coefficient magnitude degrades further, suggesting the acceleration in the prevailing active failure mechanism or the introduction of a different failure mechanism between 1000 and 2000 thermal cycles.

Reliability analysis performed on the 34 test samples, using a failure criterion of 20% average degradation in the magnitude of the transmission coefficient of the as-received data are shown in Fig. 8. From this graph, it is observed that for a maximum frequency of 20 GHz that the highest failure rate

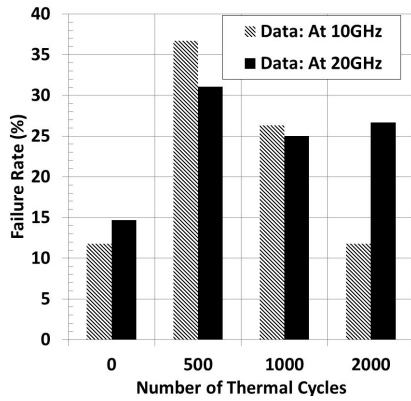


Fig. 8. Reliability analysis data showing the relationship between failure rate and the number of thermal cycles at 10 and 20 GHz frequencies.

occurs after 500 thermal cycles for both 10 GHz (37%) and 20 GHz (31%) data. Afterward, the sample failure rate is subsequently observed to steadily decrease at 10 GHz, while it seems to saturate at 20 GHz. This suggests that the high failure rate at 500 thermal cycles could be because of the initiation of defects and their subsequent propagation.

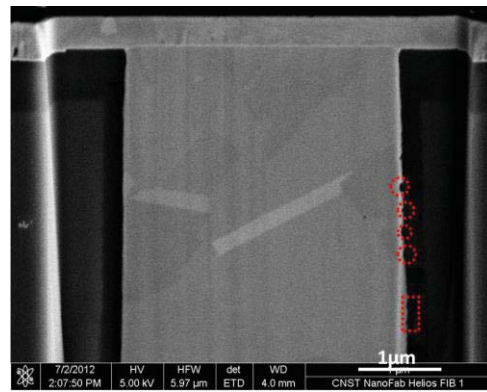
Although the failure rate at 10 GHz is observed to decrease consistently after the initial 500 cycles, at 20 GHz the failure rate seems to saturate after the initial 500 cycles. This decrease in failure rate after the initial 500 thermal cycles, suggests a decrease in defect generation and their propagation in the TSV daisy chain.

On the other hand, early failures are also observed in the TSV daisy chain structure, with failure rates of 12% and 15% at 10 and 20 GHz, respectively. These early failures are attributed to processing-related issues that results in chip-to-chip variability in the RF signal characteristics within a wafer.

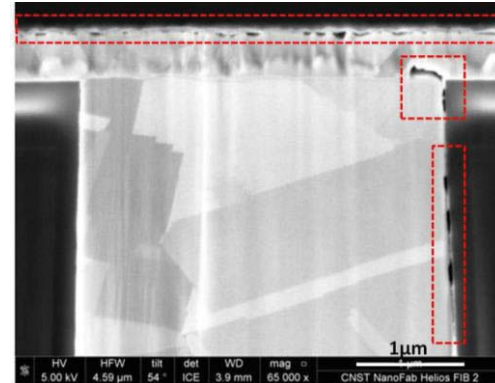
B. FIB-Based

To understand the root causes of the observed changes in the RF characteristics of the TSV chain with thermal cycling, FIB-based cross-sectional SEM images of the TSVs for the as-received and the 1000 thermal-cycled test conditions are performed and shown in Fig. 9. For the as-received sample [Fig. 9(a)], pinhole voids are only observed at the sidewall interface between Cu and the TaN barrier layer. On the other hand, the 1000 thermal-cycled sample [Fig. 9(b)] show a lot of large voids in three different locations. Voids are observed to propagate within the M1 layer. Additionally, large voids are observed at the Cu TSV-TaN interface, as well as at the Cu TSV-M1 interface. The voids at the Cu TSV-TaN interface are observed to link up with the Cu TSV-M1 voids after 1000 thermal cycles.

Fig. 9 SEM images confirm that thermal cycling results in the growth and propagation of defects, specifically, voids, as discussed earlier. Therefore, the formation and propagation of voids are the cause of the decrease in the magnitude of the transmission coefficient with thermal cycling. The voids increase the damping in the structure, as they also act as scattering centers for RF signals.



(a)



(b)

Fig. 9. FIB-based SEM cross-sectional images of the top region of the TSV and its connecting metal layer (M1); (a) As-received state and (b) after 1000 thermal cycles. The highlighted areas: location of defects in the form of voids.

As the R_{dc} -based technique is only sensitive to defects in the conducting paths; it may not be able to detect the observed voids at the Cu TSV-TaN interface shown in Fig. 9. On the other hand, the RF-based method is sensitive to distortions in conductors, dielectrics, and semiconductors, thus, it can detect all the defects at the various locations identified in Fig. 9. This makes it a preferred technique for accessing TSV reliability performance.

IV. CONCLUSION

In this paper, the effect of thermal cycling on signal integrity in TSV chains was studied using RF-based technique. This was achieved by performing RF measurements as a function of frequency and number of thermal cycles (cumulative thermal history). RF signal was found to be an effective probe for the assessment of the effect of thermal cycling on the reliability of TSV stacked dies.

The magnitude and phase of the transmission and the reflection coefficients were studied, and the magnitude of the transmission coefficient was found to show the best correlation between the RF signal characteristics and the number of thermal cycles.

It was found that the signal integrity of the TSV daisy chain degraded with increasing number of thermal cycles. This trend was attributed to the presence of defects in the structure caused by cyclic stressing during thermal cycling. The generated voids increased the damping in the structure, as they also acted as

scattering centers for RF signals. FIB-based physical failure analysis revealed that thermal cycling resulted in the growth of voids.

The RF characteristics of the transmission coefficient magnitude for the as-received and the 500-cycled test conditions were very similar with a constant 0.4-dB decrease across all studied frequency after 500 thermal cycles. However, after 1000 and 2000 thermal cycles, the RF characteristics were observed to be significantly different from the as-received test condition, as the transmission coefficient magnitude degraded with frequency. Above 20 GHz, a drastic deterioration of the transmission coefficient magnitude was observed. This suggested that for high-frequency applications > 20 GHz, the TSVs lost its fidelity after 1000 or more number of thermal cycles.

From the reliability analysis of the TSV daisy chain, early failures were observed at time-zero, which were attributed to process variations across the wafer. This was supported by FIB-based cross-sectional SEM image, which showed pinhole voids at the Cu TSV-TaN interface, in the as-received state. The highest failure rate was observed at 500 cycles, which was suspected because of the initiation of defects and their subsequent propagation in the structure.

ACKNOWLEDGMENT

The authors would like to thank Prof. R. Geer from the College of Nanoscale Science and Engineering, State University of New York at Albany, NY, USA, and his group for the design of the RF test structure used in this paper. They would also like to thank Dr. J. Schumacher of NIST for the presented FIB images.

REFERENCES

- [1] C. Okoro, M. Gonzalez, B. Vandeveld, B. Swinnen, G. Eneman, S. Stoukatch, E. Beyne, and D. Vandepitte, "Analysis of the induced stresses in silicon during Thermocompression Cu-Cu bonding of Cu-through-vias in 3D-SiC architecture," in *Proc. 57th Electron. Compon. Technol. Conf.*, Jun. 2007, pp. 249–255.
- [2] C. Okoro, C. Huyghebaert, J. Van Olmen, R. Labie, K. Lambrinou, B. Vandeveld, E. Beyne, and D. Vandepitte, "Elimination of the axial deformation problem of Cu-TSV in 3D integration," in *Proc. 11th Int. Workshop, AIP Conf. Stress-Induced Phenomena Metall.*, vol. 1300. Nov. 2010, pp. 214–220.
- [3] O. Luhn, C. Van Hoof, W. Ruythooren, and J.-P. Celis, "Filling of microvia with an aspect ratio of 5 by copper electrodeposition," *Electrochim. Acta*, vol. 54, no. 9, pp. 2504–2508, 2009.
- [4] B. Swinnen, W. Ruythooren, P. De Moor, L. Bogaerts, L. Carbonell, K. De Munck, B. Eyckens, S. Stoukatch, D. Sabuncuoglu Tezcan, Z. Tokei, J. Vaes, J. Van Aelst, and E. Beyne, "3D integration by Cu-Cu thermo-compression bonding of extremely thinned bulk-Si die containing 10 μm pitch through-Si vias," in *Proc. IEEE Int. Electron Devices Meeting*, Dec. 2006, pp. 371–374.
- [5] A. Mercha, G. Van der Plas, V. Moroz, I. De Wolf, P. Asimakopoulos, N. Minas, S. Domae, D. Perry, M. Choi, A. Redolfi, C. Okoro, Y. Yang, J. Van Olmen, S. Thangaraju, D. Sabuncuoglu Tezcan, P. Soussan, J. H. Cho, A. Yakovlev, P. Marchal, Y. Travalay, E. Beyne, S. Biesemans, and B. Swinnen, "Comprehensive analysis of the impact of single and arrays of through silicon vias induced stress on high-k/metal gate CMOS performances," in *Proc. Int. Electron Devices Meeting*, San Francisco, CA, USA, Dec. 2010, pp. 2.2.1–2.2.4.
- [6] C. Okoro, Y. Yang, B. Vandeveld, B. Swinnen, D. Vandepitte, B. Verlinden, and I. De Wolf, "Extraction of the appropriate material property for realistic modeling of through-silicon-vias using μ -Raman spectroscopy," in *Proc. Int. Interconnect Technol. Conf.*, San Francisco, CA, USA, May 2008, pp. 16–18.

- [7] T. Frank, C. Chappaz, P. Leduc, L. Arnaud, F. Lorut, S. Moreau, A. Thuaire, R. El Farhane, and L. Anghel, "Resistance increase due to electromigration induced depletion under TSV," in *Proc. IEEE Int. Rel. Phys. Symp.*, Apr. 2011, pp. 3F.4.1–3F.4.6.
- [8] T. Frank, C. Chappaz, P. Leduc, L. Arnaud, S. Moreau, A. Thuaire, R. El Farhane, and L. Anghel, "Reliability approach of high density through silicon via (TSV)," in *Proc. 60th Electron. Compon. Technol. Conf.*, Las Vegas, NV, USA, Jun. 2010, pp. 321–324.
- [9] M. G. Farooq, T. L. Graves-Abe, W. F. Landers, C. Kothandaraman, B. A. Himmel, P. S. Andry, C. K. Tsang, E. Sprogis, R. P. Volant, K. S. Petrarca, K. R. Winstel, J. M. Safran, T. D. Sullivan, F. Chen, M. J. Shapiro, R. Hannon, R. Liptak, D. Berger, and S. S. Iyer, "3D copper TSV integration, testing and reliability," in *Proc. Int. Electron Devices Meeting*, Washington, DC, USA, Dec. 2011, pp. 7.1.1–7.1.4.
- [10] D. Kwon, M. H. Azarian, and M. G. Pecht, "Detection of solder joint degradation using RF impedance analysis," in *Proc. 58th Electron. Compon. Technol. Conf.*, Lake Buena Vista, FL, USA, May 2008, pp. 606–610.
- [11] S. Foley, L. Floyd, and A. Mathewson, "A novel fast technique for detecting voiding damage in IC interconnects," *Microelectron. Rel.*, vol. 40, no. 1, pp. 87–97, 2000.
- [12] C. Bermond, L. Cadix, A. Farcy, T. Lacrevez, P. Leduc, and B. Flechet, "High frequency characterization and modeling of high density TSV in 3D integrated circuits," in *Proc. 13th Signal Propag. Interconnects*, Strasbourg, France, May 2009, pp. 1–7.
- [13] Z. Xu and J.-Q. Lu, "High-speed design and broadband modeling of through-strata-vias (TSVs) in 3D integration," *IEEE Trans. Compon., Packag. Manuf. Technol.*, vol. 1, no. 2, pp. 154–162, Feb. 2011.
- [14] J. Kim, J. S. Pak, J. Cho, E. Song, J. Cho, H. Kim, T. Song, J. Lee, H. Lee, K. Park, S. Yang, M.-S. Suh, K.-Y. Byun, and J. Kim, "High-frequency scalable electrical model and analysis of a through silicon via (TSV)," *IEEE Trans. Compon., Packag. Manuf. Technol.*, vol. 1, no. 2, pp. 181–195, Feb. 2011.
- [15] "Maximum RF input power of SiGe: C bipolar transistor BFR740L3RH," Infineon Technologies AG, Neubiberg, Germany, Tech. Rep. TR151, Aug. 2009, pp. 1–7.
- [16] A. Sekiguchi, J. Koike, S. Kamiya, M. Saka, and K. Maruyama, "Void formation by thermal stress concentration at twin interfaces in Cu thin films," *Appl. Phys. Lett.*, vol. 79, no. 9, pp. 1264–1266, 2001.



Chukwudi Okoro received the Ph.D. degree in mechanical engineering from Katholieke Universiteit Leuven, Leuven, Belgium in 2010.

He has been with the National Institute of Standards and Technology, Gaithersburg, MD, USA as a Post-Doctoral Scientist since 2011.



Pavel Kabos received the Ph.D. and D.Sc. (Habilitation) degrees from the Slovak University of Technology, Bratislava-Old Town, Slovakia, in 1979 and 1994, respectively.

He is a Staff Physicist, Electromagnetics Division, National Institute of Standards and Technology, Boulder, CO, USA.



Jan Obrzut received a Ph.D. degree in Technical Sciences from Cracov Polytechnic, Kraków, Poland.

He is with National Institute of Standards and Technology, Gaithersburg, MD, USA, researching metrology of dielectric films and hybrid materials for microwave and electronic applications.



Dr. Yaw S. Obeng has over 20 years of proven technical leadership in corporate, entrepreneurial and academic environments.

He is currently the Leader of the Back-End-of-Line Reliability Project, Physical Measurement Laboratory, National Institute of Standards and Technology, Gaithersburg, MD, USA.



Klaus Hummler is a Senior Principal Engineer and Program Manager of the 3D Integration, Test Vehicles, and Reliability Program in SEMATECH's Interconnect Division, Albany, NY, USA, which focuses on new interconnect technologies for tomorrow's advanced computer chips.